AD-A040 229 ARMY ARMAMENT RESEARCH AND DEVELOPMENT COMMAND WATER--ETC F/G 20/11
THE EFFECT OF AUTOFRETTAGE ON FATIGUE CRACK PROPAGATION IN EXTE--ETC(U)
MAY 77 J A KAPP

UNCLASSIFIED ARLCB-TR-77025 NL

| OF |
ADA
040229

END
DATE
FILMED
6-77

(12)

ARLCB

TECHNICAL REPORT ARCLB-TR-77025

THE EFFECT OF AUTOFRETTAGE ON FATIGUE CRACK PROPAGATION IN EXTERNALLY FLAWED THICK-WALLED DISKS

J. A. KAPP

MAY 1977

US ARMY ARMAMENT RESEARCH AND DEVELOPMENT COMMAND
LARGE CALIBER WEAPON SYSTEM LABORATORY
BENÉT WEAPONS LABORATORY
WATERVLIET, N. Y. 12189

use

AMCMS No. 3110.15.0003

PRON No. 32-6-P4957

APPROVED FOR PUBLIC RELEASE; DISTRIBUTION UNLIMITED

DISCLAIMER

The findings in this report are not to be construed as an official Department of the Army position unless so designated by other authorized documents.

The use of trade name(s) and/or manufacturer(s) in this report does not constitute an official indorsement or approval.

DISPOSITION

Destroy this report when it is no longer needed. Do not return it to the originator.

SECURITY CLASSIFICATION OF THIS PAGE (When Data Entered)

REPORT DOCUMENTATION PAGE

READ INSTRUCTIONS BEFORE COMPLETING FORM

1. REPORT NUMBER: (14) ARLCB-TR-77025	2. GOVT ACCESSION NO.
3. RECIPIENT'S CATALOG NUMBER	(9) Technical rept.
4. TITLE (and Subtitle): (6) The Effect of Autofrettage on Fatigue Crack Propagation in Externally Flawed Thick-walled Disks.	5. TYPE OF REPORT & PERIOD COVERED
	6. PERFORMING ORG. REPORT NUMBER
7. AUTHOR(s): (10) J. A. Kapp	8. CONTRACT OR GRANT NUMBER(s)
9. PERFORMING ORGANIZATION NAME AND ADDRESS: Benet Weapons Laboratory, Watervliet Arsenal, Watervliet, N.Y. 12189, DRDAR-LCB-TL	10. PROGRAM ELEMENT, PROJECT, TASK AREA & WORK UNIT NUMBERS: AMCMS No. 3110.15.0003; PRON No. 32-6-P4957
11. CONTROLLING OFFICE NAME AND ADDRESS: US Army Armament Research and Development Command, Large Caliber Weapon System Laboratory, Dover, New Jersey 07801	12. REPORT DATE: (11) May 1977
	13. NUMBER OF PAGES: ~~44~~ (12) 48p.
14. MONITORING AGENCY NAME & ADDRESS (if different from Controlling Office)	15. SECURITY CLASS. (of this report): UNCLASSIFIED
	15a. DECLASSIFICATION/DOWNGRADING SCHEDULE

16. DISTRIBUTION STATEMENT (of this Report)

Approved for public release; distribution unlimited.

17. DISTRIBUTION STATEMENT (of the abstract entered in Block 20, if different from Report)

18. SUPPLEMENTARY NOTES

This report was presented as a thesis for Graduate Studies.

19. KEY WORDS (Continue on reverse side if necessary and identify by block number)

Pressure vessels	Fatigue	Fracture Mechanics
Autofrettage	Stress Analysis	NASTRAN

20. ABSTRACT (Continue on reverse side if necessary and identify by block number)

The effect of the autofrettage residual stress distribution on the crack growth rate in externally flawed thick-walled disks has been investigated. The crack growth rate was modeled by using the Paris power law relation. Stress intensity factors were calculated for internally pressurized, externally flawed, non-autofrettaged cylinders, by an approximate technique and with the use of the NASTRAN finite element computer program. A simple experiment was devised to determine the effect of autofrettage on crack growth rate. The the test involved diametrically loading thin disks,

(See Other Side)

DD FORM 1 JAN 73 1473 EDITION OF 1 NOV 65 IS OBSOLETE

410 224

SECURITY CLASSIFICATION OF THIS PAGE (When Data Entered)

20. cut from autofrettaged cylinders. NASTRAN was used to determine the stress intensity factors for this loading geometry. The experimentally observed results show that autofrettage increases the crack growth rate in externally flawed cylinders, but the test did not supply sufficient data to mathematically model the increase. The faster crack growth rate is believed to be caused by the local relaxation of the tensile autofrettage residual stresses due to large plastic zones accompanying crack growth.

TABLE OF CONTENTS

LIST OF ILLUSTRATIONS

LIST OF ILLUSTRATIONS (Cont)

LIST OF TABLES

NOTATION

a - Inside radius of a cylinder or disk

A_σ - Area under a stress distribution

b - Outside radius of a cylinder or disk

B - Wall thickness (b-a)

c - Crack depth

c_f - Final crack depth

c_i - Initial crack depth

dA_σ - Differential area under a stress distribution

F - Applied force

Fx, Fy - Forces in a coordinate direction

I - Moment of inertia

K_I - Stress intensity factor

ΔK_I - Range of stress intensity factor during a fatigue cycle

$M_{A'}$ - Moments about point A'

M_B - Bending moment

N - Arbitrary number of cycles

N_f - Number of cycles to failure

N_i - Number of cycles to initiate a crack to c_i

P_i - Internal pressures

ΔP_i - Range of internal pressure during a fatigue cycle

r - Polar coordinate

$\bar{r}, \bar{r}'$ - Centroids of stress distributions

NOTATION (Cont)

r_{NA} - Coordinate position of a neutral axis

t - Thickness of a disk specimen

y - Distance from the neutral axis

$Y[\frac{c}{B}]$ - Arbitrary function of non-dimensional crack depth

σ_{APP} - Applied stress

σ_{bend} - Bending stress

σ_R - Autofrettage residual stress

σ_t - Total tangential stress near a crack tip

σ_{tbend} - Bending tangential stress near a crack tip

σ_{tmod} - Modified tangential stress

$\sigma_{t\infty}$ - Tangential stress in an uncracked cylinder

σ_y - Yield stress

σ_* - Residual stress due to tensile yielding at a crack tip

Ψ - Arbitrary function of autofrettage parameters

C_1, m - Material constants

$(\sigma_{min}/\sigma_{max})$ - Stress ratio

I. INTRODUCTION

The traditional structure used in containing very high pressures is the thick-walled cylinder. The solution for the stress in these vessels was developed by Lamé and is documented in most primary texts in Strength of Materials[1]. The Lamé solution reveals that the highest tensile stressed area in thick-walled cylinders is the inside (bore) radius. To reduce the bore stress, several techniques have been developed to induce compressive residual stresses at the bore and thus increase the pressure that can be withstood elastically. They are multi-layer construction, autofrettage and wrapping[2]. The primary concern of this report is the autofrettage method.

Autofrettage is a process where a thick walled cylinder is subjected to a pressure sufficient to cause yielding in the cylinder. The pressure is then released and the cylinder recovers. Since the outside portion of the cylinder was subjected to small amounts of strain, it will try to return to nearly its original dimension, while the bore is subjected to relatively large plastic strain, and will try to remain deformed. This non-uniform recovery causes a compressive residual stress at the bore and a tensile residual stress at the outside radius. Figure 1 is a plot of some typical autofrettage residual stress distributions.

TYPICAL AUTOFRETTAGE RESIDUAL STRESS DISTRIBUTIONS

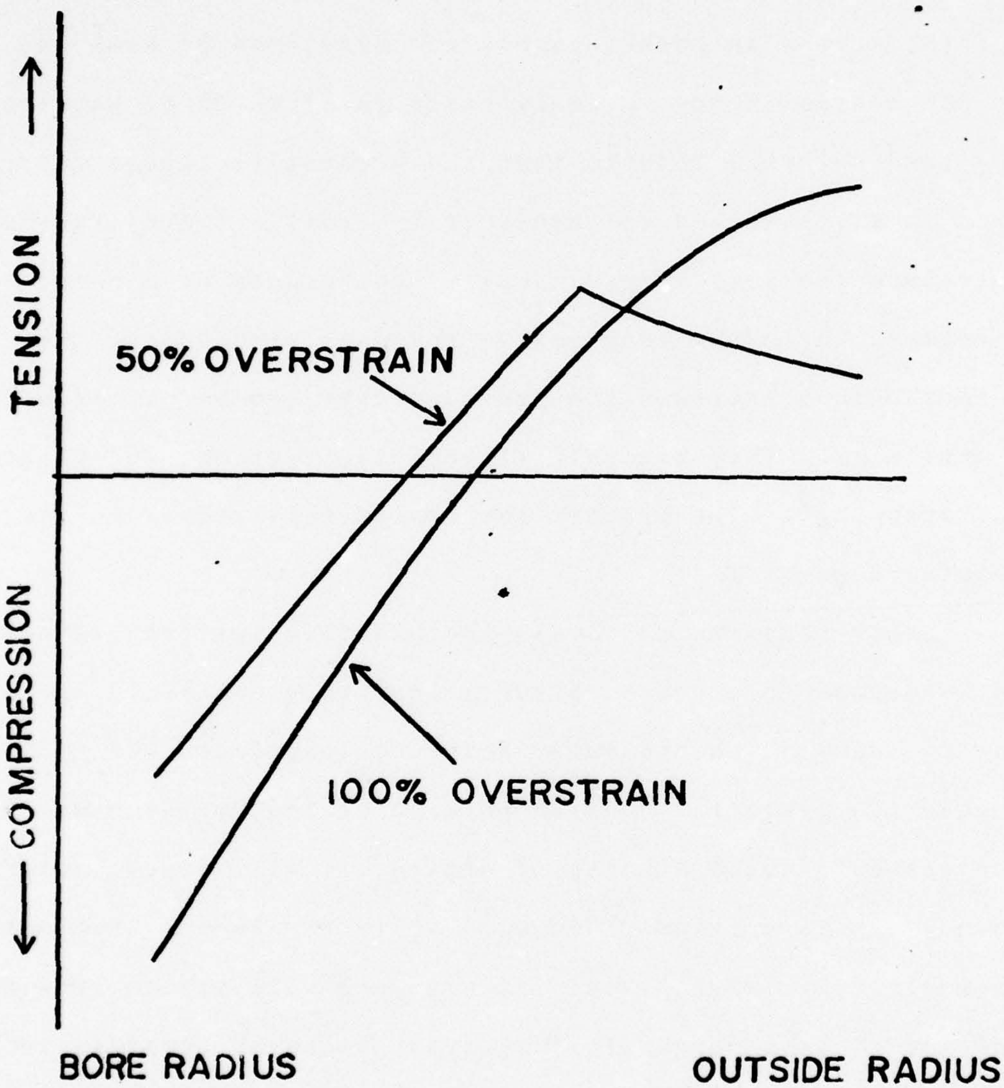

FIGURE 1.

The maximum compressive residual bore stress is obtained when the autofrettage pressure is sufficient for the outside radius to yield. This is called the 100% overstrain condition*. This condition allows for the maximum pressure to be contained elastically and has traditionally been considered the optimum design condition. If an autofrettaged cylinder is subjected to fatigue, the optimum autofrettage condition may not be 100% overstrain. The combination of tensile residual stress and tensile operating stress at the outside radius may cause crack initiation at this surface. This report is the result of an investigation of the effects of the autofrettage residual stress distribution on crack propagation initiating from flaws at the outside radius.

II. APPROACH

In order to model the effect of autofrettage on external flaw initiated fatigue crack propagation, a model must first be developed for the crack propagation in a cylinder that has not been autofrettaged. This can be accomplished with the use of linear elastic fracture mechanics, and the Paris power law for crack propagation[3]:

$$\frac{dc}{dN} = C_1 \Delta K_I^m \tag{1a}$$

---

*Percent overstrain is defined as the percentage of the wall thickness that is subjected to plastic strain during autofrettage.

Since the primary purpose for modeling crack growth is to determine remaining fatigue life, equation 1a can be integrated to:

$$(N_f - N_i) = \int_{c_i}^{c_f} \frac{dc}{C_1 \Delta K^m} \qquad (1b)$$

It is assumed that autofrettage will have an effect on crack propagation. This effect may be modeled by the following modification to the power law:

$$\frac{dc}{dN} = \Psi C_1 \Delta K^m, \qquad (2a)$$

where Ψ is an arbitrary function of autofrettage parameters determined from experiment. Once Ψ is known, an expression for the remaining fatigue life of an autofrettaged cylinder can be determined by integrating equation 2a:

$$(N_f - N_i) = \int_{c_i}^{c_f} \frac{dc}{\Psi C_1 \Delta K^m} \qquad (2b)$$

Based on the above rationale, it was planned to model the crack propagation by determining stress intensity factors at various crack depths in non-autofrettaged, externally flawed thick-walled cylinders subjected to internal pressure. It

was also planned to determine the function Ψ by performing the simple experiment discussed below.

III. THEORY

Several investigators have attempted to determine the stress intensity factors for an externally flawed cylinder subjected to internal pressure. Kobayashi[4], Chopra[5], and Kobayashi et al[6], have found the stress intensity factors in thin-walled cylinders using various techniques. Emery and Segedin[7] have determined the stress intensity factors for cylinders of wall thickness to inside radius ratio (B/a), varying from .052 to 1.85 using a finite difference method. While this method yields good results for some loading and specimen geometries, it gives poor results in others. It was therefore decided to develop an expression for the stress intensity factor using another method.

One assumption that can be made is that a single external crack in a thick-walled cylinder will produce the same stress intensity factor as that encountered in a single edge notched panel. The stress intensity factor can then be approximated by[8]:

$$K_I = 1.12\sigma\sqrt{c\pi} , \qquad (3)$$

where σ is the stress normal to the plane crack, in the vicinity of the crack.

The problem then reduces to evaluating the tangential stress in the uncracked ligament of wall thickness. This stress can be approximated based on the following assumptions:

1. The cylinder is infinitely long and open-ended.

2. The crack is oriented in the radial direction and is of constant depth for the entire length of cylinder.

3. The tangential stress distribution ($\sigma_{t\infty}$), 180° removed from the crack is unaffected by the presence of the crack and is given by the Lamé solution[1].

$$\sigma_{t\infty} = \frac{P_i a^2}{b^2 - a^2} \left[1 + \frac{b^2}{r^2}\right] \tag{4}$$

4. The tangential stress distribution in the uncracked ligament of wall thickness (σ_{tmod}) is given by the Lamé solution for an uncracked cylinder whose outside radius has been reduced by the crack depth:

$$\sigma_{tmod} = \frac{P_i a^2}{(b-c)^2 - a^2} \left[1 + \frac{(b-c)^2}{r^2}\right] \tag{5}$$

5. The stresses are symmetric about the plane of the crack. The first two assumptions reduce the analysis to a two-

dimensional problem. The third is an evocation of the St. Venant Principle. The fourth is a "uniform thinning" approximation that has been used successfully in analyzing internally cracked cylinders[9], and the last is based on the geometry of a cracked cylinder. These assumptions are represented schematically in Figure 2a.

The stability of a cylinder subjected to the above assumed loading can then be determined by analyzing its free body diagram, Figure 2b. It is readily observed that the cylinder is in translational equilibrium. Since the resultant forces of the stress distributions act eccentric to the resultant force of the pressure distribution, a moment (M_B) must act over the uncracked thickness for rotational equilibrium to be maintained. The value of M_B per unit length of cylinder can be shown to be:

$$M_B = P_i a^2 \left[\frac{b^2}{b^2 - a^2} \ln \left[\frac{b}{a}\right] - \frac{(b-c)^2}{(b-c)^2 - a^2} \ln \left[\frac{b-c}{a}\right] \right] \qquad (6)$$

The total tangential stress distribution in the uncracked wall thickness therefore, has two components: 1) the modified Lamé stress and 2) a bending stress due to M_B ($\sigma_{t\ bend}$). The bending stress can be found based on[1]:

$$\sigma_{t\ bend} = \frac{M_B y}{I}\ , \qquad (7a)$$

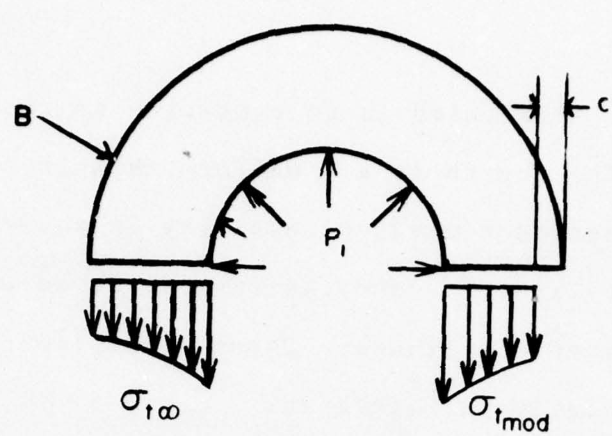

Figure 2a. Schematic of assumed stress distribution of an externally flawed, thick-walled cylinder, subjected to internal pressure

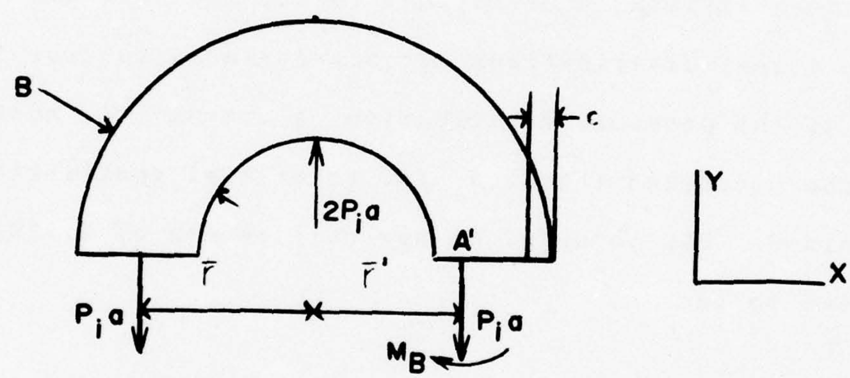

Figure 2b. Free body diagram of an externally flawed, thick-walled cylinder, subjected to internal pressure

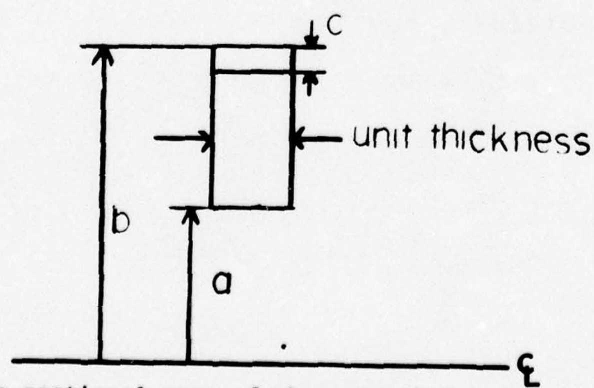

Figure 2c. Cross-sectional area of the uncracked ligament of wall thickness

where y is the distance from the neutral axis and I is the moment of inertia. Since the area over which M_B acts is rectangular as shown in Figure 2c, the bending stress in this case is:

$$\sigma_{t\,bend} = \frac{12P_i a^2[r-\frac{(b-c+a)}{2}]}{(b-c-a)^3}\left[\frac{b^2}{b^2-a^2}\ln[\frac{b}{a}] - \frac{(b-c)^2}{(b-c)^2-a^2}\ln[\frac{b-c}{a}]\right] \quad (7b)$$

The total tangential stress distribution is therefore given by the sum of equations 7b and 5:

$$\sigma_t = P_i a^2\left\{\frac{1}{(b-c)^2-a^2}[1+\frac{(b-c)^2}{r^2}] + \frac{12(r-\frac{(b-c+a)}{2})}{(b-c-a)^3}\left[\frac{b^2}{b^2-a^2}\ln\left[\frac{b}{a}\right] - \frac{(b-c)^2}{(b-c)^2-a^2}\ln\left[\frac{b-c}{a}\right]\right]\right\} \quad (8)$$

To check the accuracy of equation 8, it was decided to utilize the finite element program NASTRAN. A grid was generated, using linear elements, to model a cylinder of 4 units outside radius and 2 units inside radius, for a B/a ratio of 1. The grid is illustrated in Figure 3. Cracks of various depths were modeled by running the program several times. On each successive run, the constraint on the row of grid points marked A-A was reduced, which allowed the unrestrained points to act as a free surface. The NASTRAN

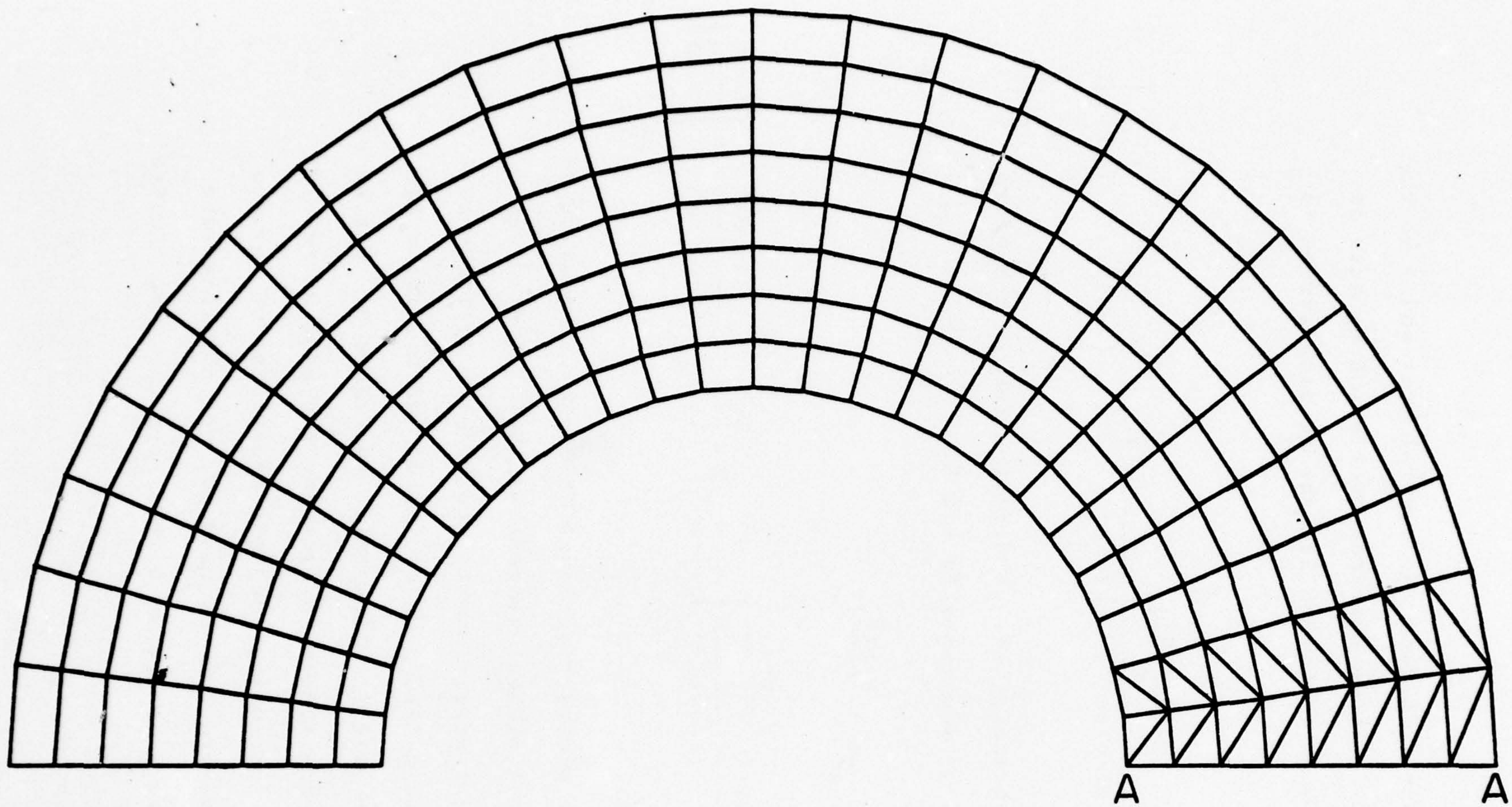

FIGURE 3. LINEAR FINITE ELEMENT GRID

COMPARISON OF THE DERIVED AND NASTRAN PREDICTED TANGENTIAL STRESS NEAR THE ROOT OF THE CRACK

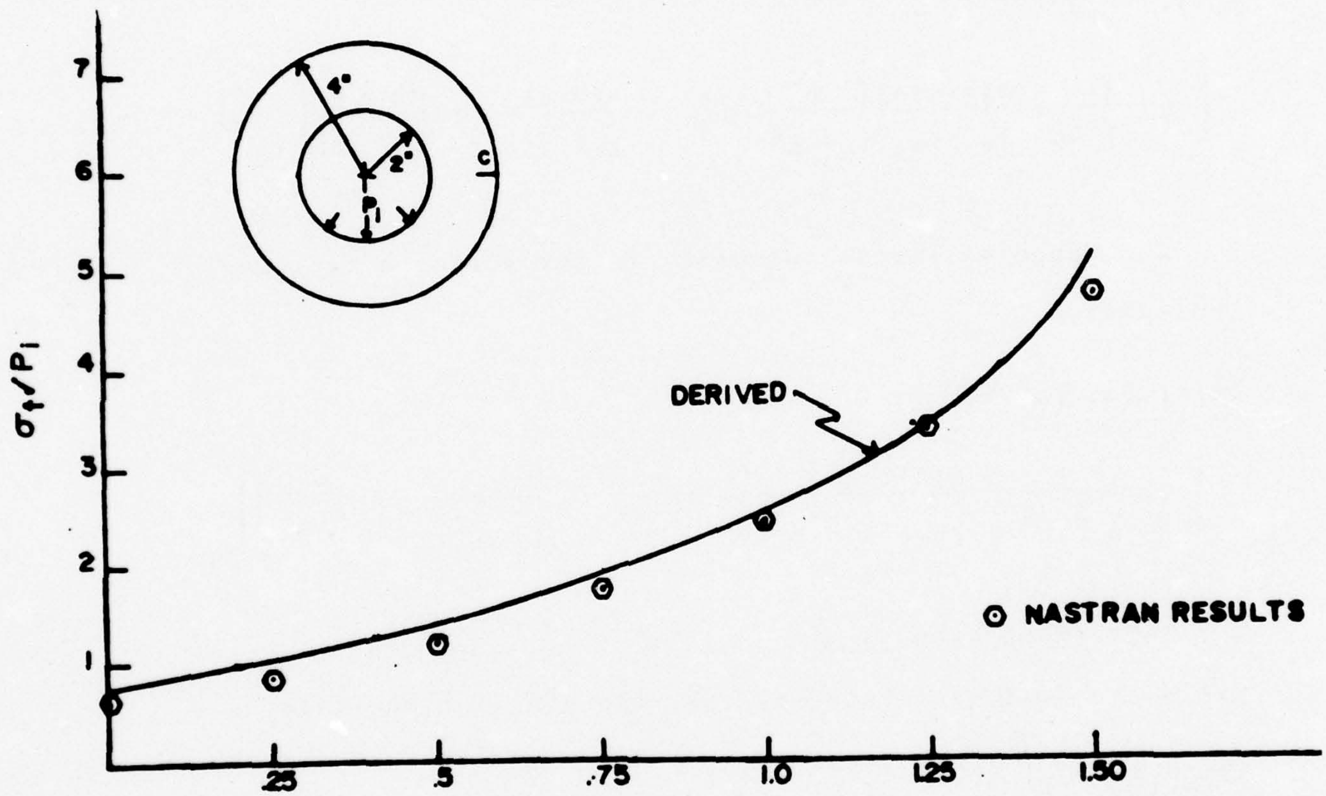

FIGURE 4.

predicted stresses are plotted in Figure 4 and show excellent agreement with equation 8.

The stress intensity factor is determined by substituting the quantity (b-c) for r in equation 8, and using this value of σ_t for σ in equation 3:

$$K_I = 1.12 P_i a^2 \sqrt{\pi c}$$

$$\left[\frac{2}{(b-c)^2 - a^2} + \frac{6(b-c+a)}{(b-c-a)^3}\left[\frac{b^2}{b^2-a^2}\ln\left[\frac{b}{a}\right] - \frac{(b-c)^2}{(b-c)^2-a^2}\ln\left[\frac{b-c}{a}\right]\right]\right] \quad (9)$$

The range of stress intensity factor during a fatigue cycle is:

$$\Delta K_I = 1.12 \Delta P_i a^2 \sqrt{\pi c}$$

$$\left[\frac{2}{(b-c)^2 - a^2} + \frac{6(b-c+a)}{(b-c-a)^3}\left[\frac{b^2}{b^2-a^2}\ln\left[\frac{b}{a}\right] - \frac{(b-c)^2}{(b-c)^2-a^2}\ln\left[\frac{b-c}{a}\right]\right]\right] \quad (10)$$

This expression is substituted in equation 1b, to yield the following integral for remaining fatigue life:

$$(N_f - N_i) = \frac{1}{C_1}\int_{c_i}^{c_f} \left\{1.12 \Delta P_i a^2 \sqrt{\pi c}\right.$$

$$\left.\left[\frac{2}{(b-c)^2 - a^2} + \frac{6(b-c+a)}{(b-c-a)^3}\left[\frac{b^2}{b^2-a^2}\ln\left[\frac{b}{a}\right] - \frac{(b-c)^2}{(b-c)^2-a^2}\ln\left[\frac{b-c}{a}\right]\right]\right]\right\}^{-m} dc \quad (11)$$

Since equation 11 can only be integrated by approximation, it was decided to develop an analytical expression for remaining fatigue life, by determining the stress intensity factors by another method. A recent study by Hussain et al[10] has found that stress intensity factors can be predicted very accurately and efficiently by using quadratic finite elements in the NASTRAN program.

The element is basically a trapezoid that is defined as the connection of eight grid points, (four corner points and four mid-side points) as shown in Figure 5a. If one side of the trapezoid is defined as connecting two corner and one mid-side points, all having the same coordinate position, these points define one corner of a triangle as shown in Figure 5b. If the adjacent mid-side points are then placed one fourth of the distance between the remaining corners of the triangle, the numerical expressions for the stresses and strains at these mid-side points are singular of order one half ($1/\sqrt{r}$), which is the same order of singularity that occurs in the Westergaard near field solution[11]. These elements can therefore be used to very accurately model a crack. The stresses or strains predicted by NASTRAN, using these elements, are substituted in the Westergaard solution to solve for the stress intensity factor. This method has

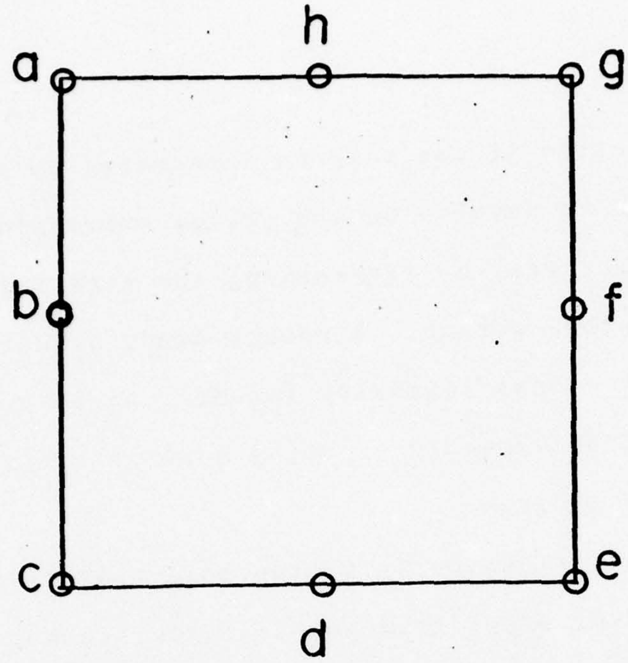

FIGURE 5a QUADRATIC ELEMENT

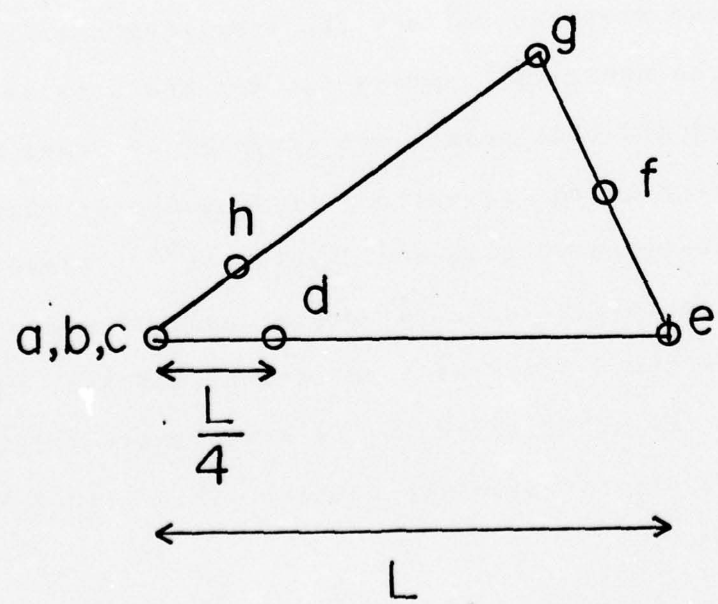

FIGURE 5b SINGULAR ELEMENT

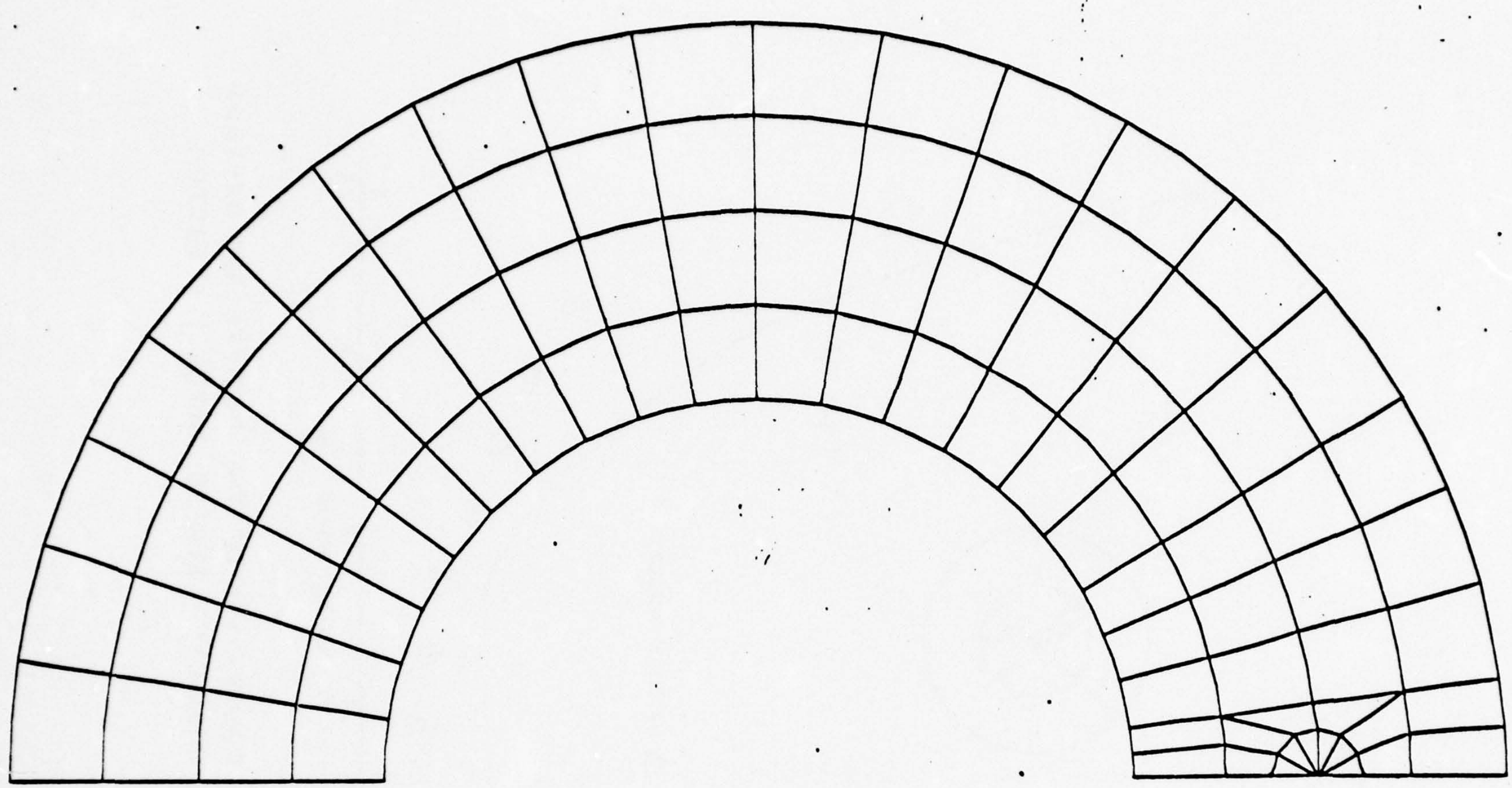

FIGURE 6 QUADRATIC FINITE ELEMENT GRID

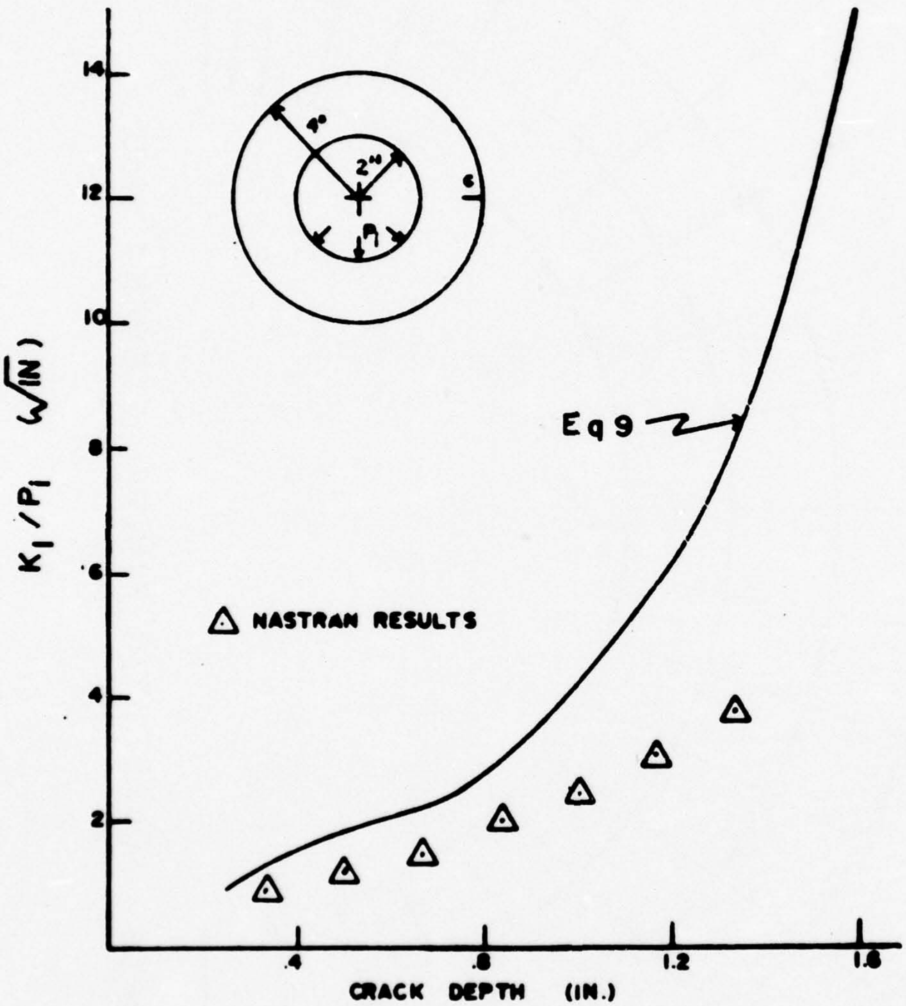

FIGURE 7 COMPARISON OF THE DERIVED AND NASTRAN PREDICTED STRESS INTENSITY FACTOR

predicted stress intensity factors for several geometries within 2-3%[10]. Figure 6 is a grid with six singular elements.

Stress intensity factors were found for nine crack depths. The results are compared with equation 9 in Figure 7. The plot shows that equation 9 predicts stress intensity factors much greater than the NASTRAN prediction for deep cracks. A deviation from equation 9 can be expected for deep cracks, since it was derived from equation 2, which was developed assuming that the crack depth is negligible in comparison with the size of the medium in which it is embedded[8]. For very shallow cracks, the assumption is valid, but for deep cracks it does not hold; therefore, the NASTRAN predictions are believed to be far more accurate than equation 9.

To fully utilize the NASTRAN data, it was decided to fit a curve to them. An equation of the following type was assumed:

$$K_I = \sigma \sqrt{B}\, Y[\tfrac{c}{B}] \ , \qquad (12a)$$

where σ is a stress far removed from the crack.

For the case of internal pressure loading σ was chosen as the tangential stress at the outside radius 180° removed

from the crack ($\sigma = \sigma_{t\infty}$ @($r=b$)). The expression for the stress intensity factor becomes:

$$K_I = \frac{2P_i a^2}{b^2-a^2} \sqrt{B}\, Y \left[\frac{c}{B}\right] \tag{12b}$$

The arbitrary function $Y[\frac{c}{B}]$ is found by linear regression. The best fit is accomplished by the fourth degree polynomial:

$$Y\left[\frac{c}{B}\right] = .5687 + 18.3132\left[\frac{c}{B}\right]^2 - 32.7075\left[\frac{c}{B}\right]^3 + 25.5121\left[\frac{c}{B}\right]^4 \tag{13a}$$

This function has a correlation coefficient (R^2) of .9999.

When equations 13a and 12b are substituted in equation 1a to predict remaining fatigue life, the resulting expression is very cumbersome to integrate.

A good fit can also be obtained by the quadratic:

$$Y\left[\frac{c}{B}\right] = .6916 + 8.1217\left[\frac{c}{B}\right]^2 \tag{13b}$$

which has a correlation coefficient of .9911.

Substituting equation 13b into equation 12b the following is obtained:

$$K_I = \frac{2P_i a^2}{b^2-a^2} \sqrt{B}\, \left(.6916 + 8.1217\left[\frac{c}{B}\right]^2\right) \tag{14}$$

The range of stress intensity factor during a fatigue cycle is given by:

$$\Delta K_I = \frac{2\Delta P_i a^2}{b^2-a^2} \sqrt{B} \quad (.6916 + 8.1217[\frac{c}{B}]^2) \tag{15}$$

When equation 15 is substituted in equation 1b, the expression can be integrated in closed form for integer values of Paris power law exponents m. Since most steels have m values between 2 and 4, the integration has been performed for m = 2,3 and 4. The results of the integration are reported in Table 1. Equations 13a and 13b are compared with the NASTRAN data in Figure 8a.

The NASTRAN predicted stress intensity factors are compared with those predicted by Emery and Segedin[6] in Figure 8b. The plot shows that the NASTRAN prediction differs substantially from that predicted by Emery and Segedin for thick-walled cylinders (B/a >.5), but is still in trend agreement with their predictions for thinner walled cylinders (B/a = .111, .25). There is no reason to believe the NASTRAN data to be in error, and it is therefore assumed to be the best solution available for cylinders of B/a ratio of 1.

IV. EXPERIMENTATION

To determine the effects of the autofrettage residual

TABLE 1. Expressions for remaining fatigue life in an externally flawed, thick-walled cylinder, subjected to internal pressure for various values of Paris power law exponent

$$(N_f - Ni) = \frac{1}{C_1}\left\{\frac{2\Delta P i a^2}{(b^2-a^2)B^{3/2}}\right\}^{-m} \int_{ci}^{c_f} \frac{dc}{(.6916B^2 + 8.1217c^2)^m}$$

let $$\Phi = \frac{1}{C_I}\left\{\frac{2\ Pia^2}{(b^2-a^2)B^{3/2}}\right\}^{-m}$$

$\alpha = .6916B^2$

$\beta = 8.1217$

$m = 2$

$$(N_f - N_i) = \Phi\left[\frac{c}{2\alpha(\alpha+\beta c^2)} + \frac{1}{2\sqrt{\alpha^3}} \tan^{-1} \frac{c\sqrt{\alpha\beta}}{\alpha}\right]_{ci}^{c_f}$$

$m = 3$

$$(N_f - N_i) = \Phi\left[\frac{c(5\alpha+3\beta c^2)}{8\alpha^2(\alpha+\beta c^2)^2} + \frac{3}{8\sqrt{\alpha^5\beta}} \tan^{-1} \frac{c\sqrt{\alpha\beta}}{\alpha}\right]_{c_i}^{c_f}$$

$m = 4$

$$(N_f - N_i) = \Phi\left[\frac{c(33\alpha^2+40\alpha\beta c^2+15\beta^2c^4)}{48\alpha^3(\alpha+\beta c^2)^3} + \frac{15}{48\sqrt{\alpha^7\beta}} \tan^{-1} \frac{c\sqrt{\alpha\beta}}{\alpha}\right]_{ci}^{c_f}$$

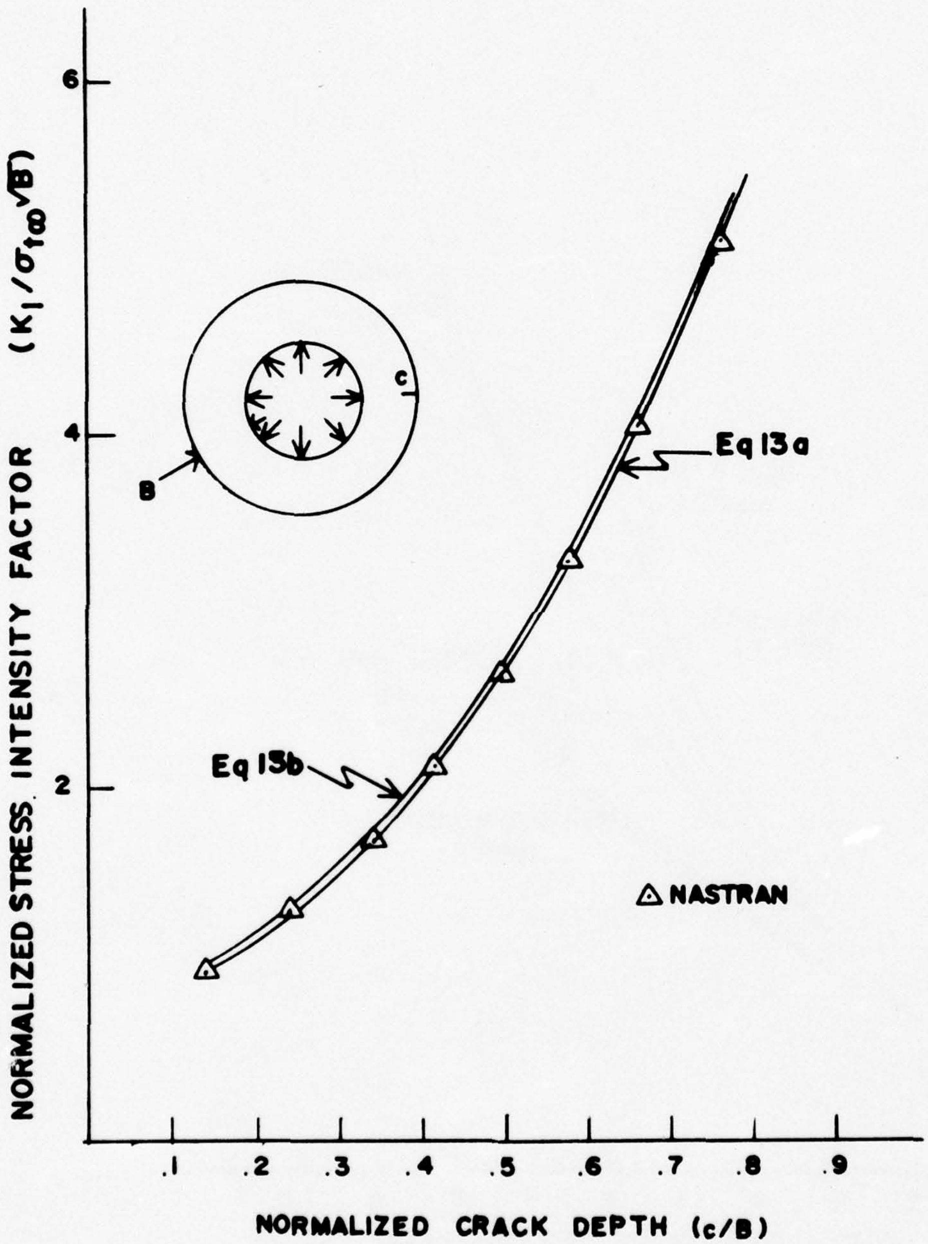

FIGURE 8a NASTRAN STRESS INTENSITY FACTORS

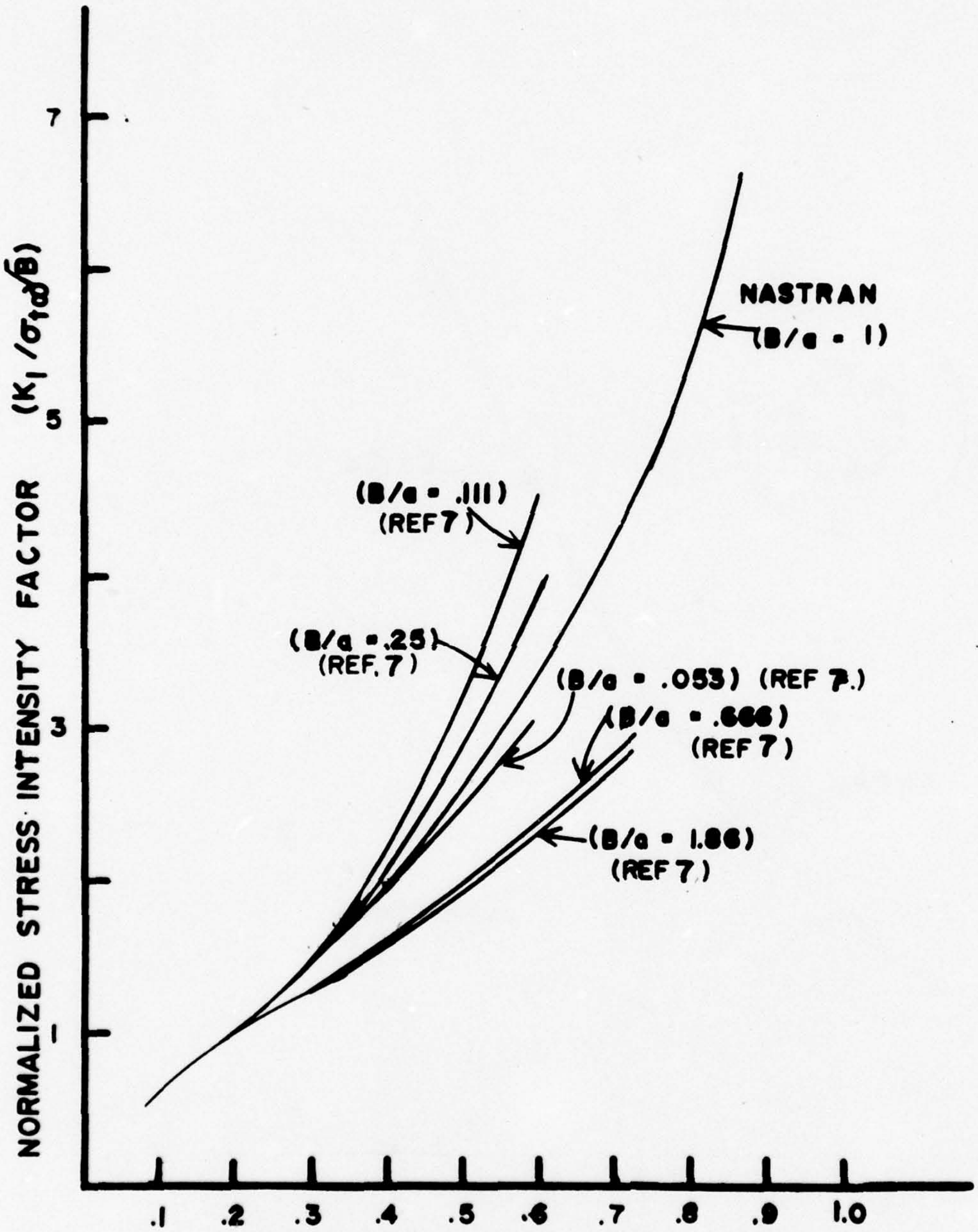

FIGURE 8b COMPARISON OF STRESS INTENSITY FACTORS

SCHEMATIC OF DISK EXPERIMENT

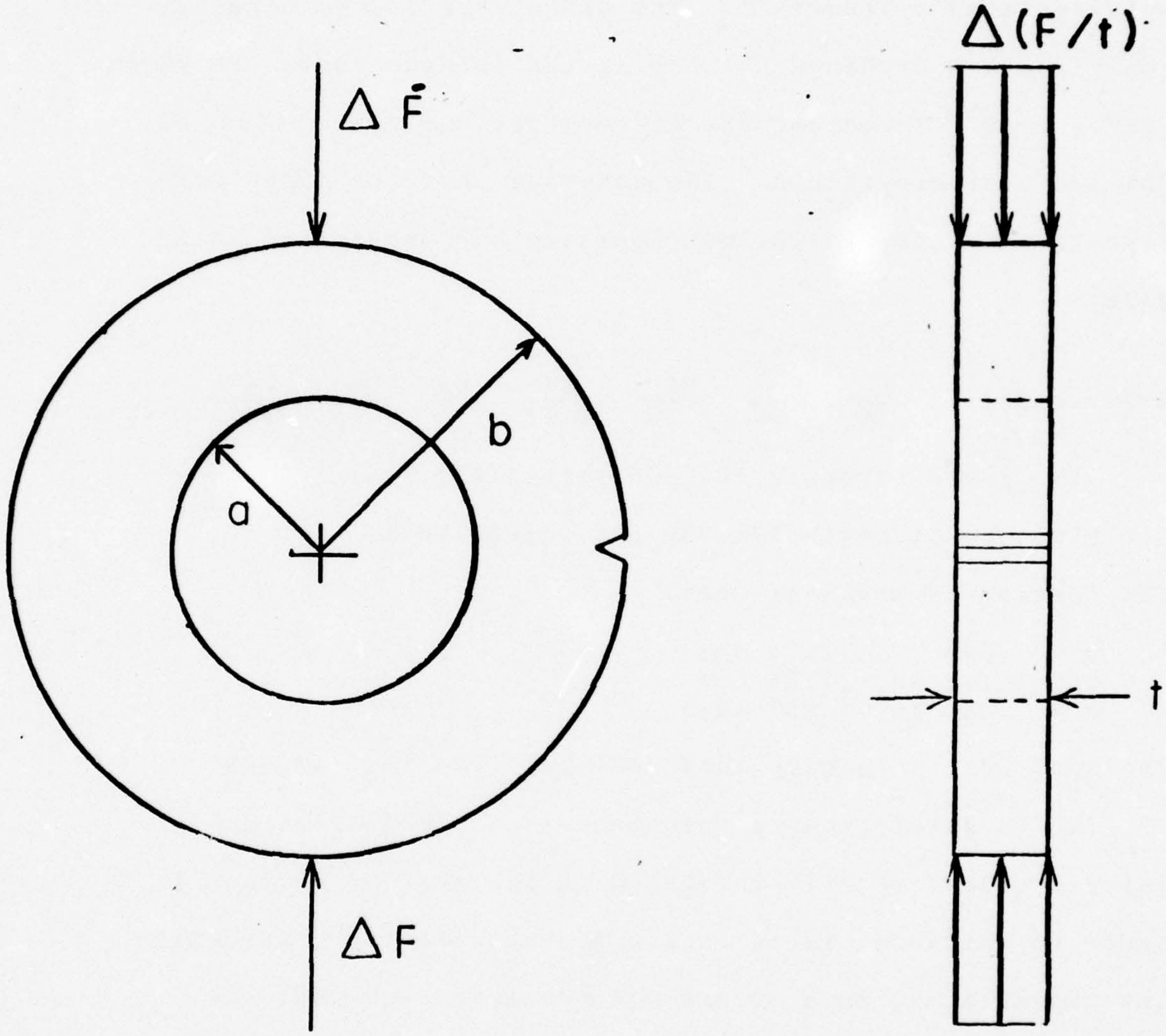

FIGURE 9

stresses on crack propagation and thus the function ψ, a simple experiment was proposed using thin disks of miniature autofrettaged cylinders[12]. The disks were loaded diametrically and had machined notches at the outside radius as shown in Figure 9. Three amounts of autofrettage were tested; 0%, 50% and 100% overstrain. The material that the disks were made from had the following chemistry and properties (AISI 4340):

% by weight	C	Mn	Si	Ni	Cr	Mo	Fe
	.39	.80	.29	1.97	.8	.25	Bal.

.1% Yield strength 166,000 psi (1144 MPa)

Ultimate strength 175,000 psi (1206 MPa)

The specimen dimensions were:

a = .604 in. (1.53 cm)
b = 1.125 in. (2.86 cm)
t = .25 in. (.635 cm)

The applied alternating load (ΔF) was 2700 lb. (12000N).

In the autofrettaged specimens (50%, 100% overstrain) fatigue cracks readily initiated at the root of notch. In order to initiate cracks in the non-autofrettaged specimens (0% overstrain), much deeper notches were required.

V. RESULTS AND DISCUSSION

To compare the results of the experiment on a c vs. N type plot, N had to be arbitrarily defined as the number of applied cycles minus the number of cycles required to

grow a crack 1/2 of the distance through the wall thickness $(N-N_{50})$. The raw c vs. $(N-N_{50})$ data is shown in Figure 10.

An interesting phenomenon occurs for very deep cracks. The crack growth rate slows in the radial direction, and the crack gradually changes direction and grows parallel to the applied alternating load. This phenomenon occurs when a crack is first subjected to Mode I and then Mode II deformations, and has been investigated by Hussain et al[13].

The loading of the disk as described, produces a compressive normal force, and a moment on the plane ahead of the crack. The moment causes a tensile bending stress sufficiently large such that the resultant of the bending and compressive normal stresses is still tensile in the outer members of the disk, in the direction perpendicular to the crack. This tensile stress causes the Mode I opening. As the crack grows, the line of action of the normal force becomes closer to the line of action of the applied force, the moment required for equilibrium therefore becomes smaller. For very deep cracks, the normal stress becomes dominant causing Mode I closure. The compressive stress then causes a shearing of the crack tip or Mode II sliding, which causes the crack to change direction.

To determine Ψ, the stress intensity factors had to be

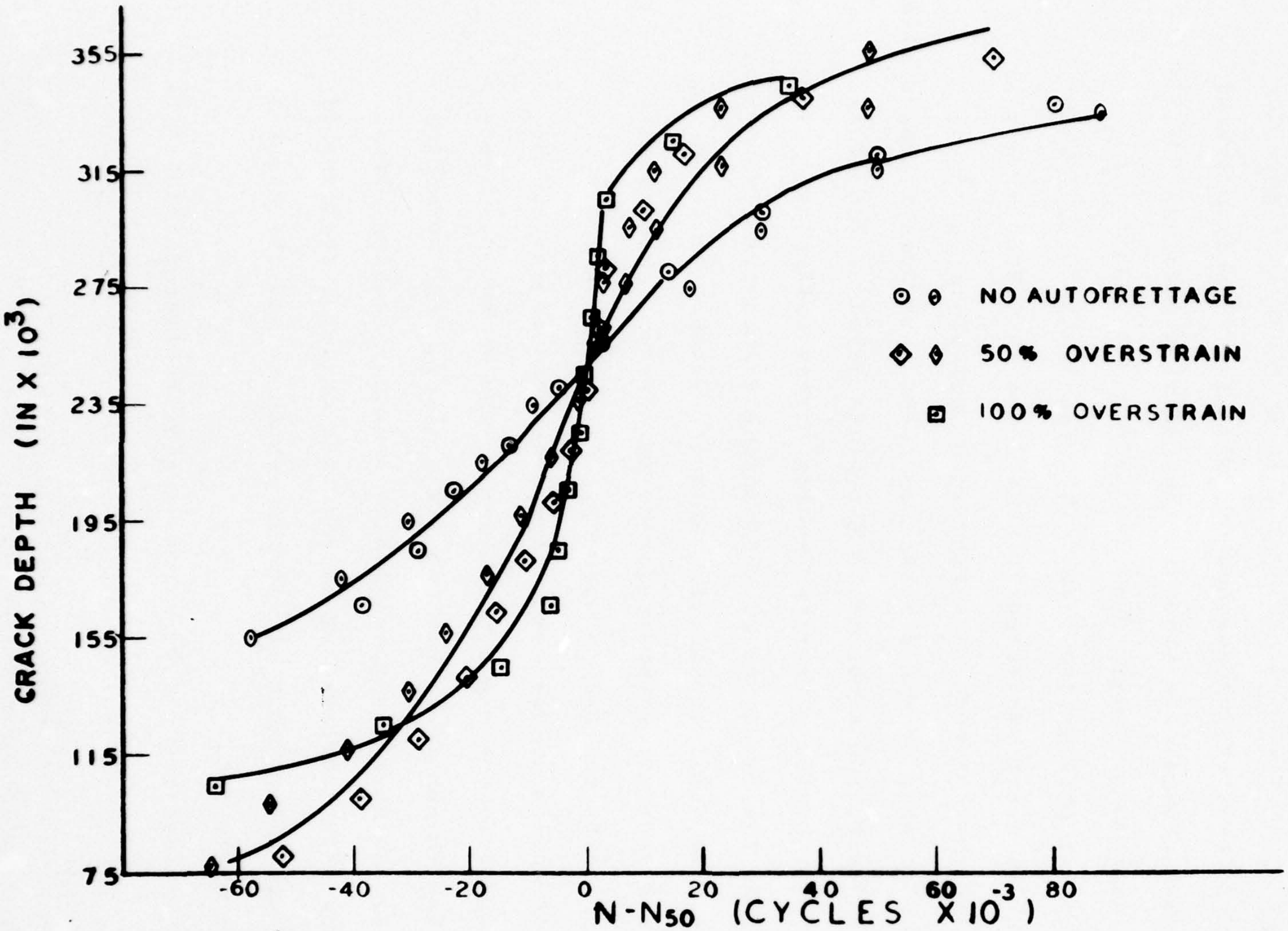

FIGURE 10 RAW DATA FROM DISK EXPERIMENT

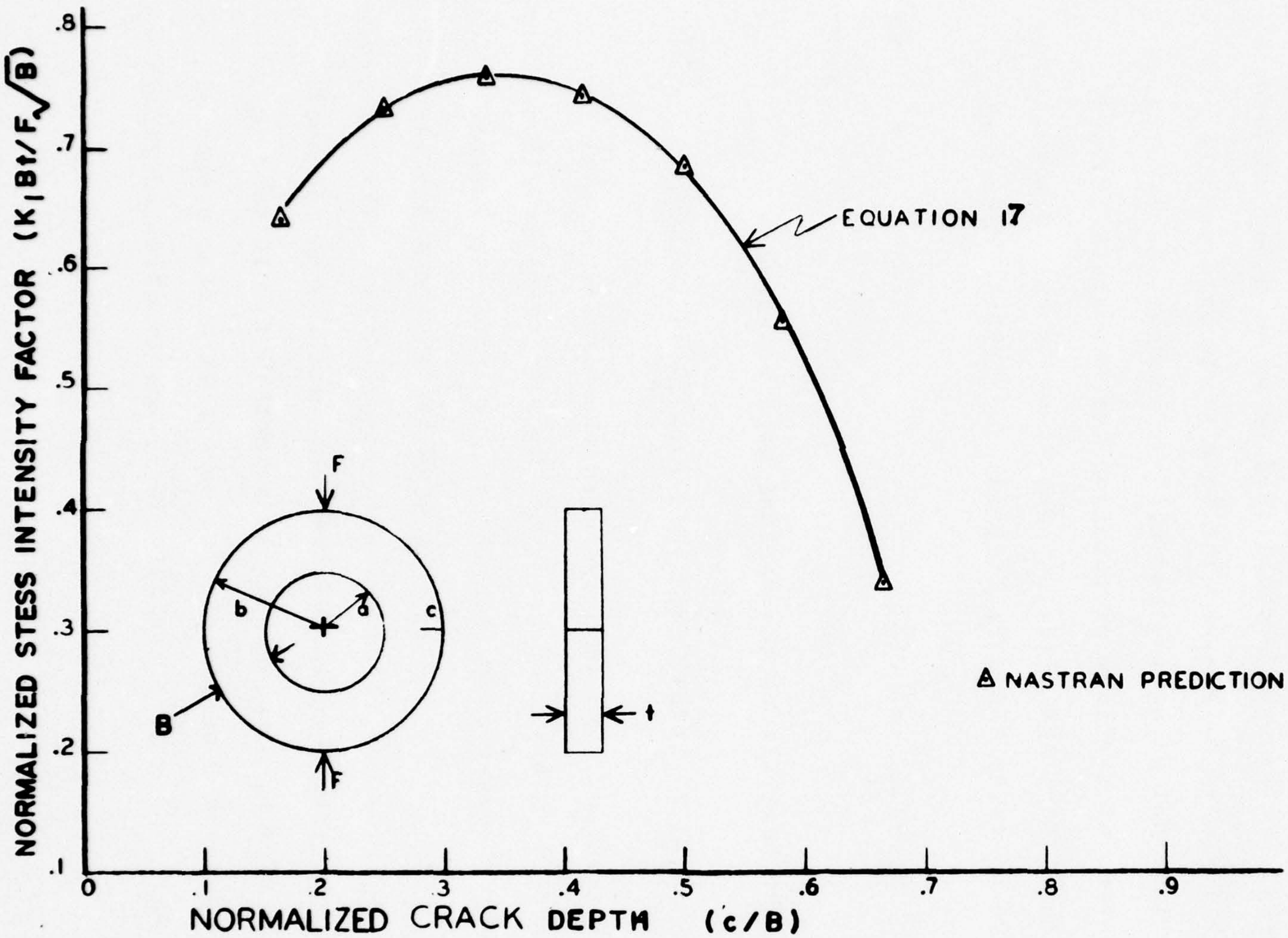

FIGURE 11 PLOT OF STRESS INTENSITY FACTORS

determined for non-autofrettaged disks under this loading geometry. This was accomplished by again using NASTRAN with singular elements. The same grids were used as with the internal pressure loading. To present the results, a relation of the form of equation 12a was again assumed. In this case, the stress σ was taken to be the absolute value of twice the normal stress (σ = F/Bt), therefore:

$$K_I = \frac{F}{Bt} \sqrt{B}\ Y[\frac{c}{B}] \tag{16}$$

The best fit to the NASTRAN data revealed:

$$Y[\frac{c}{B}] = .3625+2.1834[\frac{c}{B}]-2.8386[\frac{c}{B}]^2-1.0438[\frac{c}{B}]^4 \tag{17}$$

Equation 17 is compared with the NASTRAN results in Figure 11. This plot predicts the slow crack growth for deep cracks, because of decreasing stress intensity factor.

Equations 16 and 17 were used to develop a log dc/dN vs. log ΔK_I plot for the non-autofrettaged disks. The expected straight line behavior was not observed due to the small range of ΔK_I developed in this test ($\Delta K_I <$ 10 KSI $\sqrt{\text{in.}}$). The straight line correlation occurs at higher values of ΔK_I (20 KSI $\sqrt{\text{in.}} < \Delta K_I <$ 80 KSI $\sqrt{\text{in.}}$), and is often extrapolated

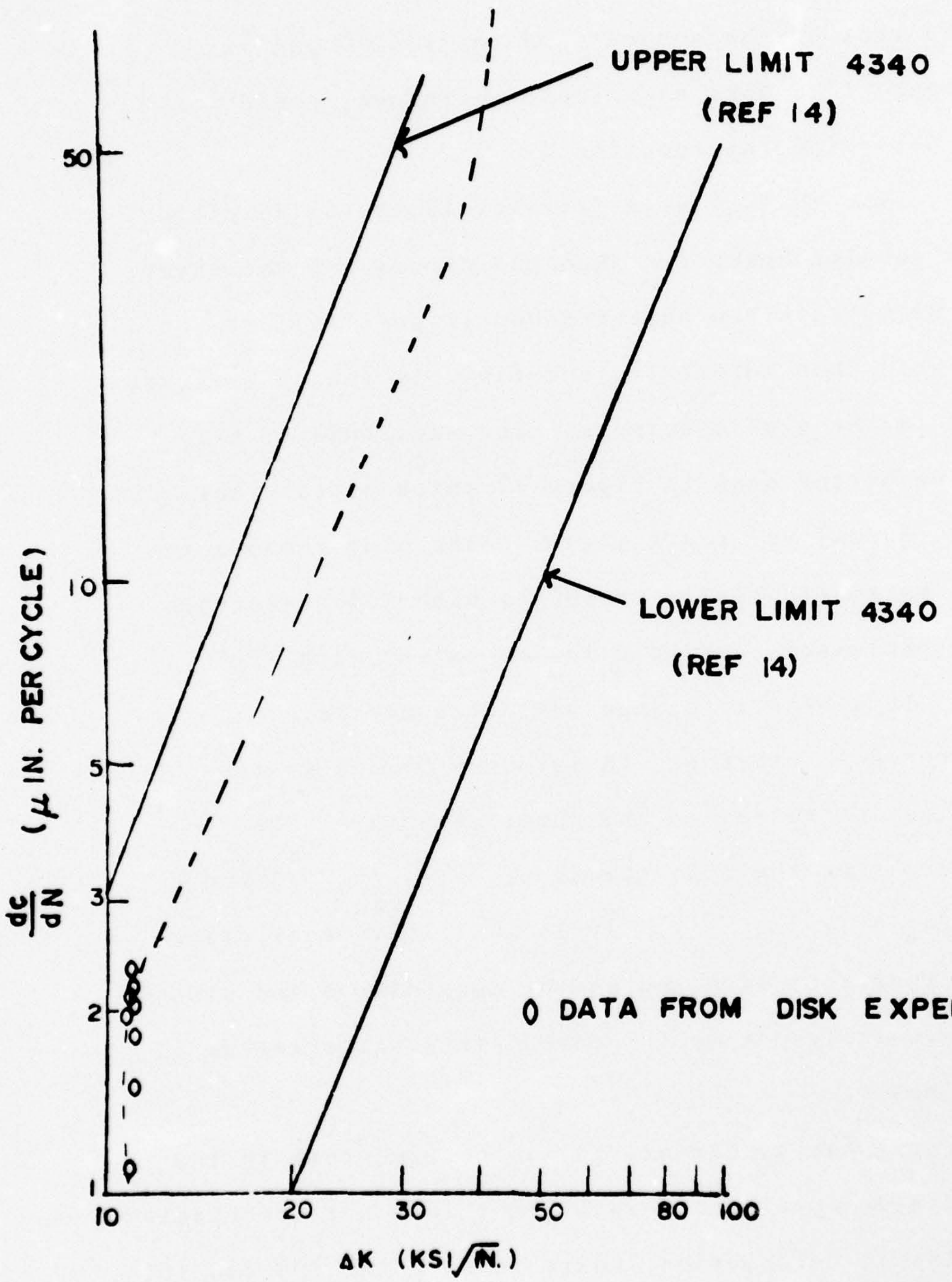

FIGURE 12 $\frac{dc}{dN}$ vs ΔK FOR THE DISK EXPERIMENT

through the lower range. The data does fall within the scatter band that has been developed for 4340[14] and is shown in Figure 12. This experiment therefore, could not be used to determine the function Ψ.

The raw c vs. $(N-N_{50})$ data (Figures 13,14,15) do yield interesting results however. When the curves for the three amounts of overstrain are superimposed (Figure 16), it can be readily seen that autofrettage definitely increases crack growth rate in the disk specimens. The magnitude of this effect can be better seen in Figure 17 which plots crack growth rate (dc/dN) vs. crack depth. The plot shows crack growth rate is substantially increased with 50% overstrain and further increased, but to a lesser extent, with 100% overstrain. This drastic change was not expected.

The increase in crack growth rate may be due to the tensile residual stresses in the outer members of the cylinder increasing the mean stress $((\sigma_{min}+\sigma_{max})/2)$ and the stress ratio $(\sigma_{min}/\sigma_{max})$. It is well known that crack growth rate increases with increasing mean stress and stress ratio, but generally not to the extent that was observed in these experiments.

In examining the specimens, it was noticed that in the non-autofrettaged specimens, crack growth was not accompanied by visual plastic deformation, while in both the 50% and 100%

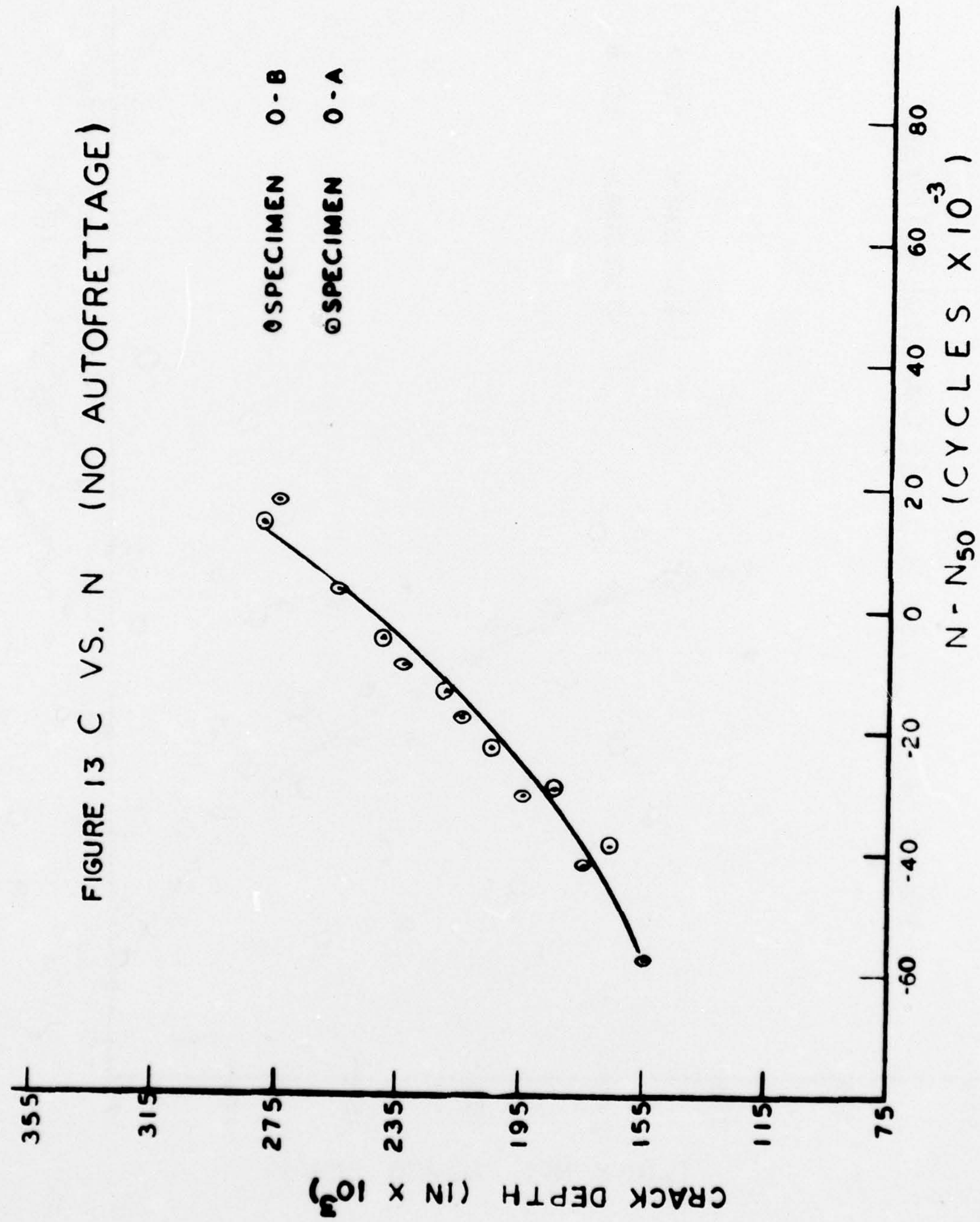

FIGURE 13 C VS. N (NO AUTOFRETTAGE)

FIGURE 14 C VS. N (50% OVERSTRAIN)

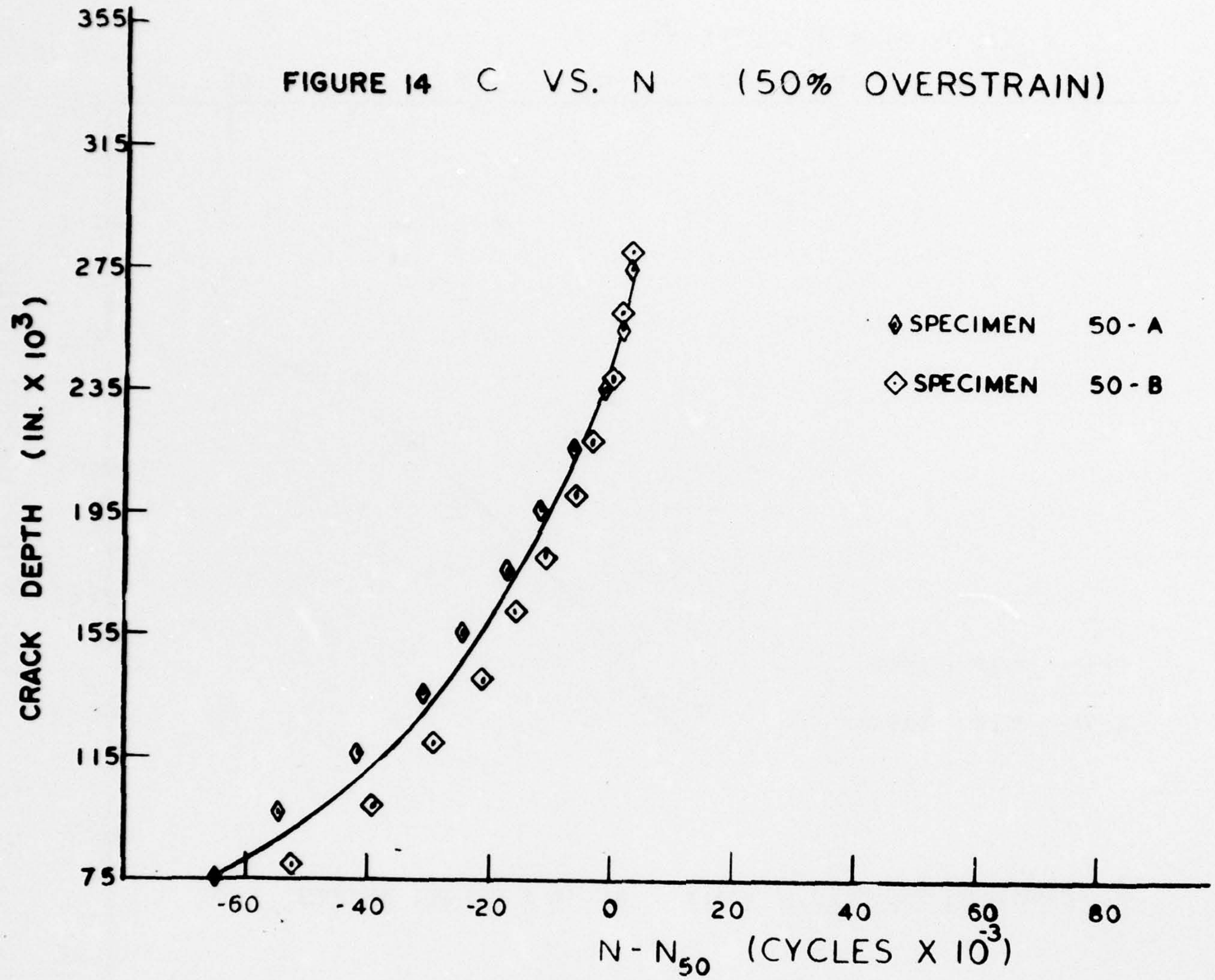

FIGURE 15 C VS. N (100% OVERSTRAIN)

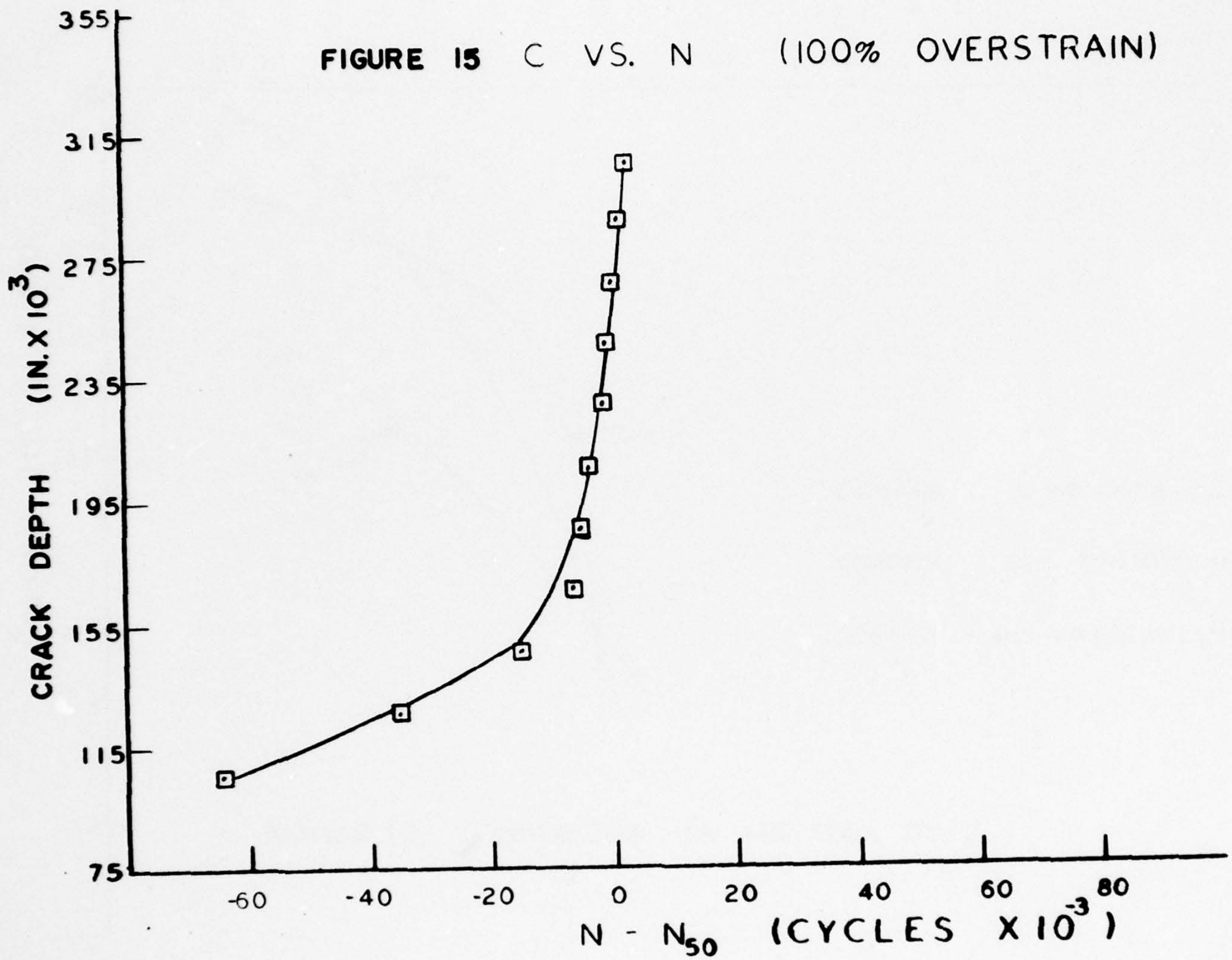

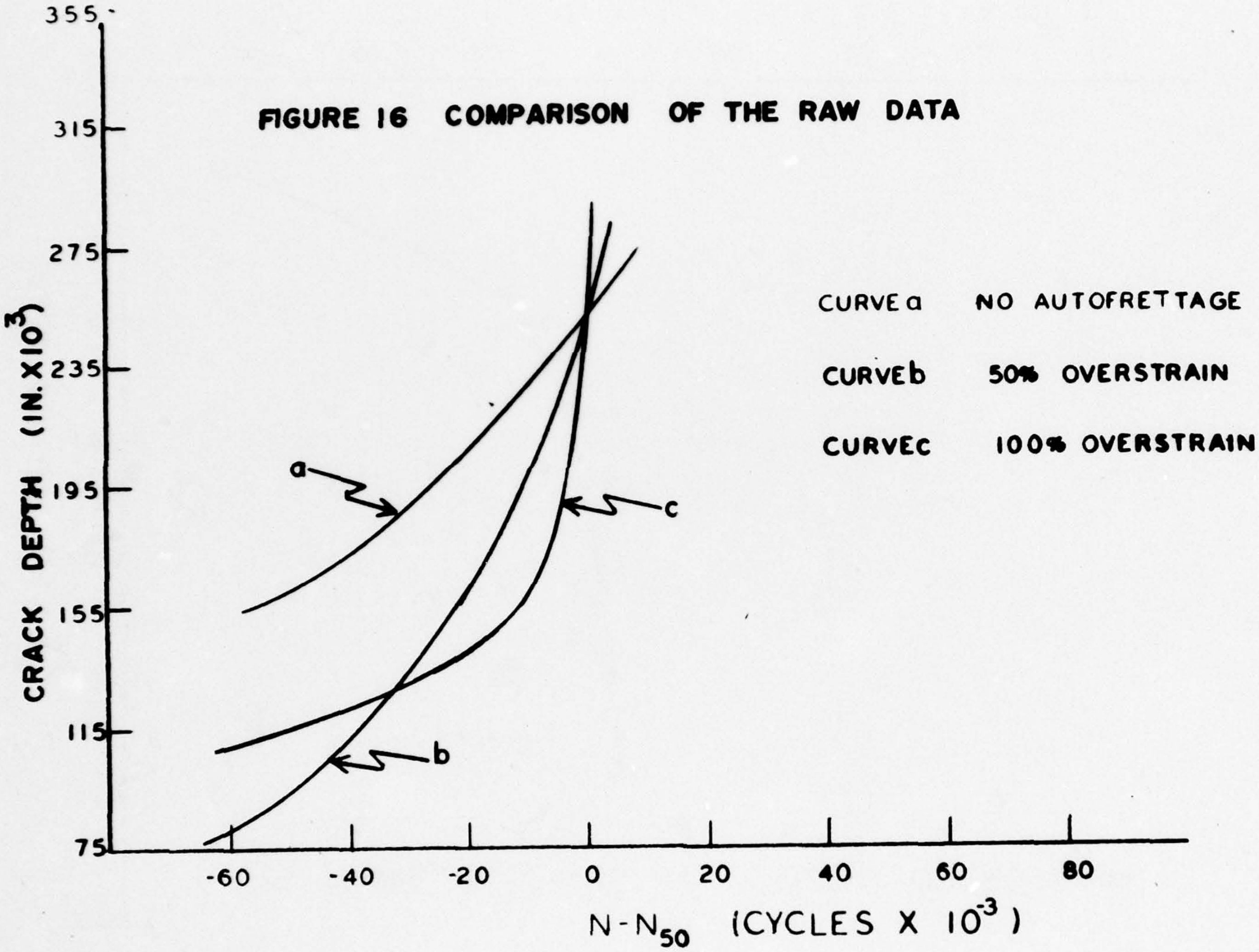

FIGURE 16 COMPARISON OF THE RAW DATA

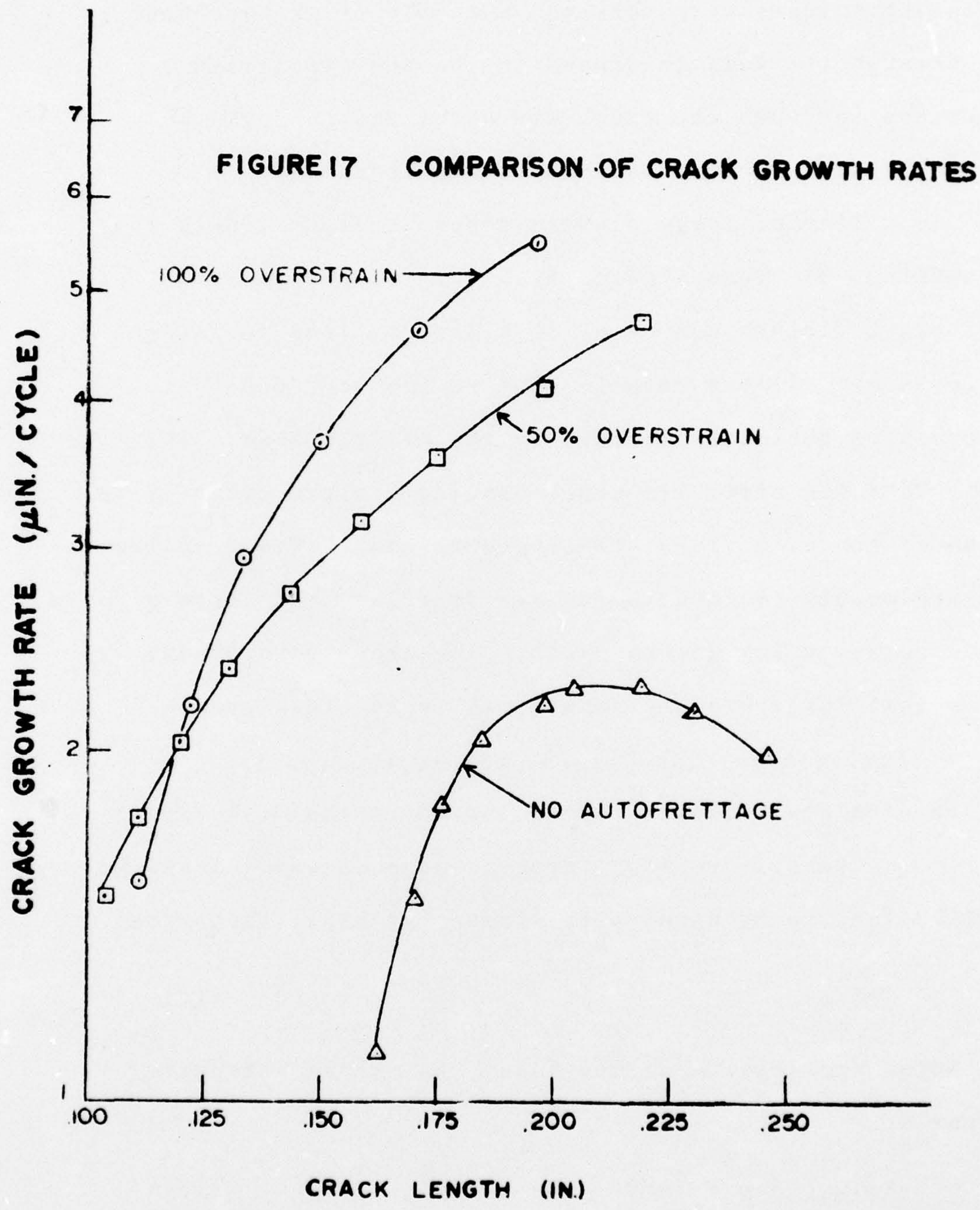

FIGURE 17 COMPARISON OF CRACK GROWTH RATES
100% OVERSTRAIN
50% OVERSTRAIN
NO AUTOFRETTAGE
CRACK GROWTH RATE (μIN. / CYCLE)
CRACK LENGTH (IN.)
1
2
3
4
5
6
7
.100
.125
.150
.175
.200
.225
.250

overstrain specimens, plastic zones were readily visible. The plastic zones were noticed when the crack was about 38% through the wall thickness in the 50% overstrain specimens and when the crack was about 31% through the wall thickness in the 100% overstrain specimens.

The effect of large plastic zones on crack growth rate in aluminum has been studied by Elber[15]. He has found that crack closure can occur in a zero to tensile fatigue cycle before all the tensile load is removed, due to the compressive residual stresses in the plastic zone. This means that the effective crack opening fatigue cycle is decreased; hence, a slower crack growth rate. Based on this closure model, the conclusion can be drawn that large plastic zones retard crack growth, yet in the above experiment, it seems that large plastic zones accelerate crack growth.

A similar model can be used to explain the accelerated crack growth that occurred in the disk experiment. The tensile residual stress causes a crack under no applied load to be open, with stress intensity factor of:

$$(K_I)_{min} \propto \sigma_R \tag{18}$$

After application of the load, the stress intensity factor is:

$$(K_I)_{max} \propto \sigma_R + \sigma_{APP} \tag{19}$$

If the sum of the residual and applied stresses exceeds the yield strength, the stress intensity factor at maximum load is:

$$(K_I)_{max} \propto \sigma_y \qquad (20)$$

When the load is removed after yielding has occurred, some of the tensile residual stress is locally relaxed by an amount σ^*, which causes the crack to close more under minimum load. The stress intensity factor at minimum load is:

$$(K_I)_{min} \propto \sigma_R - \sigma^* \qquad (21)$$

When the load is again applied, the stress intensity factor at maximum load is:

$$(K_I)_{max} \propto \sigma_R - \sigma^* + \sigma_{APP} \qquad (22)$$

If the sum of applied and residual stresses still exceed the yield strength, the stress intensity factor at maximum load again is:

$$(K_I)_{max} \propto \sigma_y \qquad (23)$$

Since the stress intensity factor at maximum load is constant (equations 20,23), but at minimum load is reduced proportional to σ^* (equation 22), the range of stress intensity factor (ΔK_I) is increased, causing faster crack growth rate. If σ^* is large enough, a large increase in crack growth

rate is expected.

Since the plastic zone appeared at shallower crack depths, and was larger in the 100% overstrain specimens than the 50% overstrain specimens, σ^* associated with 100% overstrain is expected to be larger than σ^* associated with 50% overstrain; therefore, faster crack growth rate is expected with more autofrettage.

VI. CONCLUSION

Autofrettage has a deleterious effect on fatigue crack propagation in externally flawed thick-walled cylinders. The effect is believed to be the result of a crack closure phenomenon caused by large plastic zones accompanying crack growth which effectively increases the stress intensity factor range. If the plastic zones could be reduced, by experimenting with thicker specimens, the large increase in crack growth rate would probably also be reduced.

VII. ACKNOWLEDGEMENT

The author would like to acknowledge the help of Mr. W. Mortimer for his assistance in conducting the above experiments, Mr. J. Bak for obtaining the specimens, Dr. M. Hussain, Mr. W. Lorenson and Mr. G. Pflegl, for their suggestions and assistance in the use of the program NASTRAN, and Mr. J. Underwood for his many suggestions, guidance and assistance in analyzing the data, and Mrs. M. Dietz for typing the manuscript.

REFERENCES:

1. Timoshenko, S., "Strength of Materials, Part II", Third Edition, D. Van Nostrand Co., Princeton, N.J., 1956.

2. Davidson, T.E. and Kendall, D.P., "The Design of Pressure Vessels for Very High Pressure Operation", Watervliet Arsenal Technical Report, WVT-6917, 1969.

3. Paris, P.C., "The Fracture Mechanics Approach to Fatigue" in "Fatigue, An Interdisciplinary Approach", Burke, J.J., Reed, N.L., Weiss, V., Editors, Syracuse University Press, (1964), pp 107-132.

4. Kobayashi, A.S., "A Simple Procedure for Estimating Stress Intensity Factor in Region of High Stress Gradient", Interim Technical Report No. 1, U.S. Army Research Grant No. DA-ARO-D-31-124-73-638, 1973.

5. Chopra, P.S., "Finite Element Fracture Mechanics Analysis of Creep Rupture of Fuel Element Cladding", Nuclear Engineering and Design 29, 1974.

6. Kobayashi, A.S., Maiden, D.E., and Simon, B.J., "Application of Finite Element Analysis Method to Two-Dimensional Problems in Fracture Mechanics", ASME Paper No. 69-WA/PVP-12, 1969, pp 1-7.

7. Emery, A.F. and Segedin, "The Evaluation of the Stress Intensity Factors for Cracks Subjected to Tension, Torsion, and Flexure by an Efficient Numerical Technique", Journal of Basic Engineering, pp 387-393, June 1972.

8. Wigglesworth, L.A., "Stress Distribution in a Notched Plate", Mathematica, 4 (157), 76-79.

9. Shannon, R.W.E., "Crack Growth Monitoring by Strain Sensing", Pres. Ves. and Piping (1), pp 61-73, 1973.

10. Hussain, M.A., Lorensen, W.E., and Pflegl, G., "The Quarter-Point Quadratic Isoparametric Element as a Singular Element for Crack Problems", to be published in NASA Technical Memorandum, NASTRAN: Users Experiences, October 1976.

11. Westeagaard, H.M., "Bearing Pressures and Cracks", Transactions of the ASME, Journal of Applied Mechanics, 1939.

12. Underwood, J.H., private communication, July 1976.

13. Hussain, M.A., Pu, S.L., and Underwood, J., "Strain Energy Release Rate for a Crack Under Combined Mode I and Mode II", Fracture Analysis, ASTM STP560, American Society for Testing and Materials, pp 2-28, 1974.

14. Clark, W.G., "How Fatigue Crack Initiation and Growth Properties Affect Material Selection and Design Criteria", Metals Engineering Quarterly, pp 16-22, August 1974.

15. Elber, Wolf, "The Significance of Fatigue Crack Closure", Damage Tolerance in Aircraft Structures, ASTM STP486, American Society for Testing and Materials, pp 230-242, 1971.

WATERVLIET ARSENAL INTERNAL DISTRIBUTION LIST

May 1976

	No. of Copies
COMMANDER	1
DIRECTOR, BENET WEAPONS LABORATORY	1
DIRECTOR, DEVELOPMENT ENGINEERING DIRECTORATE	1
ATTN: RD-AT	1
RD-MR	1
RD-PE	1
RD-RM	1
RD-SE	1
RD-SP	1
DIRECTOR, ENGINEERING SUPPORT DIRECTORATE	1
DIRECTOR, RESEARCH DIRECTORATE	2
ATTN: RR-AM	1
RR-C	1
RR-ME	1
RR-PS	1
TECHNICAL LIBRARY	5
TECHNICAL PUBLICATIONS & EDITING BRANCH	2
DIRECTOR, OPERATIONS DIRECTORATE	1
DIRECTOR, PROCUREMENT DIRECTORATE	1
DIRECTOR, PRODUCT ASSURANCE DIRECTORATE	1
PATENT ADVISORS	1

EXTERNAL DISTRIBUTION LIST

December 1976

1 copy to each

OFC OF THE DIR. OF DEFENSE R&E
ATTN: ASST DIRECTOR MATERIALS
THE PENTAGON
WASHINGTON, D.C. 20315

CDR
US ARMY TANK-AUTMV COMD
ATTN: AMDTA-UL
AMSTA-RKM MAT LAB
WARREN, MICHIGAN 48090

CDR
PICATINNY ARSENAL
ATTN: SARPA-TS-S
SARPA-VP3 (PLASTICS TECH EVAL CEN)
DOVER, NJ 07801

CDR
FRANKFORD ARSENAL
ATTN: SARFA
PHILADELPHIA, PA 19137

DIRECTOR
US ARMY BALLISTIC RSCH LABS
ATTN: AMXBR-LB
ABERDEEN PROVING GROUND
MARYLAND 21005

CDR
US ARMY RSCH OFC (DURHAM)
BOX CM, DUKE STATION
ATTN: RDRD-IPL
DURHAM, NC 27706

CDR
WEST POINT MIL ACADEMY
ATTN: CHMN, MECH ENGR DEPT
WEST POINT, NY 10996

CDR
HQ, US ARMY AVN SCH
ATTN: OFC OF THE LIBRARIAN
FT RUCKER, ALABAMA 36362

CDR
US ARMY ARMT COMD
ATTN: AMSAR-PPW-IR
AMSAR-RD
AMSAR-RDG
ROCK ISLAND, IL 61201

CDR
US ARMY ARMT COMD
FLD SVC DIV
ARMCOM ARMT SYS OFC
ATTN: AMSAR-ASF
ROCK ISLAND, IL 61201

CDR
US ARMY ELCT COMD
FT MONMOUTH, NJ 07703

CDR
REDSTONE ARSENAL
ATTN: AMSMI-RRS
AMSMI-RSM
ALABAMA 35809

CDR
ROCK ISLAND ARSENAL
ATTN: SARRI-RDD
ROCK ISLAND, IL 61202

CDR
US ARMY FGN SCIENCE & TECH CEN
ATTN: AMXST-SD
220 7TH STREET N.E.
CHARLOTTESVILLE, VA 22901

DIRECTOR
US ARMY PDN EQ. AGENCY
ATTN: AMXPE-MT
ROCK ISLAND, IL 61201

EXTERNAL DISTRIBUTION LIST (Cont)

1 copy to each

CDR
US NAVAL WPNS LAB
CHIEF, MAT SCIENCE DIV
ATTN: MR. D. MALYEVAC
DAHLGREN, VA 22448

DIRECTOR
NAVAL RSCH LAB
ATTN: DIR. MECH DIV
WASHINGTON, D.C. 20375

DIRECTOR
NAVAL RSCH LAB
CODE 26-27 (DOCU LIB.)
WASHINGTON, D.C. 20375

NASA SCIENTIFIC & TECH INFO FAC
PO BOX 8757, ATTN: ACQ BR
BALTIMORE/WASHINGTON INTL AIRPORT
MARYLAND 21240

DEFENSE METALS INFO CEN
BATTELLE INSTITUTE
505 KING AVE
COLUMBUS, OHIO 43201

MANUEL E. PRADO / G. STISSER
LAWRENCE LIVERMORE LAB
PO BOX 808
LIVERMORE, CA 94550

DR. ROBERT QUATTRONE
CHIEF, MAT BR
US ARMY R&S GROUP, EUR
BOX 65, FPO N.Y. 09510

2 copies to each

CDR
US ARMY MOB EQUIP RSCH & DEV COMD
ATTN: TECH DOCU CEN
FT BELVOIR, VA 22060

CDR
US ARMY MAT RSCH AGCY
ATTN: AMXMR - TECH INFO CEN
WATERTOWN, MASS 02172

CDR
WRIGHT-PATTERSON AFB
ATTN: AFML/MXA
OHIO 45433

CDR
REDSTONE ARSENAL
ATTN: DOCU & TECH INFO BR
ALABAMA 35809

12 copies

CDR
DEFENSE DOCU CEN
ATTN: DDC-TCA
CAMERON STATION
ALEXANDRIA, VA 22314

NOTE: PLEASE NOTIFY CDR, WATERVLIET ARSENAL, ATTN: SARWV-RT-TP, WATERVLIET, N.Y. 12189, IF ANY CHANGE IS REQUIRED TO THE ABOVE.